

# Fully Bioabsorbable Natural-Materials-Based Triboelectric Nanogenerators

Wen Jiang, Hu Li, Zhuo Liu, Zhe Li, Jingjing Tian, Bojing Shi, Yang Zou, Han Ouyang, Chaochao Zhao, Luming Zhao, Rong Sun, Hairong Zheng, Yubo Fan,\* Zhong Lin Wang,\* and Zhou Li\*

Implantable medical devices provide an effective therapeutic approach for neurological and cardiovascular diseases. With the development of transient electronics, a new power source with biocompatibility, controllability, and bioabsorbability becomes an urgent demand for medical sciences. Here, various fully bioabsorbable natural-materials-based triboelectric nanogenerators (BN-TENGs), *in vivo*, are developed. The “triboelectric series” of five natural materials is first ranked, it provides a basic knowledge for materials selection and device design of the TENGs and other energy harvesters. Various triboelectric outputs of these natural materials are achieved by a single material and their pairwise combinations. The maximum voltage, current, and power density reach up to 55 V, 0.6  $\mu\text{A}$ , and 21.6  $\text{mW m}^{-2}$ , respectively. The modification of silk fibroin encapsulation film makes the operation time of the BN-TENG tunable from days to weeks. After completing its function, the BN-TENG can be fully degraded and resorbed in Sprague–Dawley rats, which avoids a second operation and other side effects. Using the proposed BN-TENG as a voltage source, the beating rates of dysfunctional cardiomyocyte clusters are accelerated and the consistency of cell contraction is improved. This provides a new and valid solution to treat some heart diseases such as bradycardia and arrhythmia.


Ever-increasing neurological and cardiovascular diseases required innovation and development of implantable medical devices (IMDs).<sup>[1–4]</sup> These devices mainly include sensors, gastric and cardiac pacemakers, cardioverter defibrillators, and stimulators for the deep brain, nerves, or bone.<sup>[5–7]</sup> Long-term *in vivo* diagnosis and therapy have a very high demand on the high reliability, good biocompatibility, minimal toxicity, and miniaturization of the IMDs components. The power sources of most existing IMDs rely on rechargeable or non-rechargeable batteries.<sup>[8–10]</sup> However, the internal heat, capacity loss, and battery failure are the common problems of this kind of power source. Once these batteries finished their mission, the patients had to undergo a second operation to remove them and bear considerable financial burdens as well as severe pain. Therefore, it is urgent to develop a new method to bypass these obstacles and avoid risks of infection and inflammation under long-term implantation.<sup>[11–16]</sup>

Dr. W. Jiang, H. Li, Z. Liu, Z. Li, J. J. Tian, Dr. B. J. Shi, Y. Zou, H. Ouyang, C. C. Zhao, L. M. Zhao, Prof. Z. L. Wang, Prof. Z. Li  
CAS Center for Excellence in Nanoscience  
Beijing Institute of Nanoenergy and Nanosystems  
Chinese Academy of Sciences  
Beijing 100083, P. R. China  
E-mail: zhong.wang@mse.gatech.edu; zli@binn.cas.cn

Dr. W. Jiang, H. Li, Z. Liu, Z. Li, J. J. Tian, Dr. B. J. Shi, Y. Zou, H. Ouyang, C. C. Zhao, L. M. Zhao, Prof. Z. L. Wang, Prof. Z. Li  
School of Nanoscience and Technology  
University of Chinese Academy of Sciences  
Beijing 100049, P. R. China

H. Li, Z. Liu, Dr. B. J. Shi, Prof. Y. B. Fan  
Key laboratory for biomechanics and Mechanobiology  
of Ministry of Education  
School of Biological Science and Medical Engineering  
Beihang University  
Beijing 100083, China  
E-mail: yubofan@buaa.edu.cn

H. Li, Z. Liu, Dr. B. J. Shi, Prof. Y. B. Fan  
Beijing Advanced Innovation Centre for Biomedical Engineering  
Beihang University  
Beijing 102402, China  
Prof. R. Sun, Prof. H. R. Zheng  
Shenzhen Institutes of Advanced Technology  
Chinese Academy of Sciences  
Shenzhen 518055, China  
Prof. Z. L. Wang  
School of Materials Science and Engineering  
Georgia Institute of Technology  
Atlanta, GA 30332-0245, USA

 The ORCID identification number(s) for the author(s) of this article can be found under <https://doi.org/10.1002/adma.201801895>.

DOI: 10.1002/adma.201801895

Recently, the triboelectric nanogenerator (TENG) was proposed and has proved to be effective in converting ambient mechanical energy to electrical energy.<sup>[17–20]</sup> The conversion mechanism depends on the coupling between triboelectric effect and electrostatic induction. This emerging technology provided an alternative solution for battery-less electronic devices. Previous researches demonstrated that the TENGs have superior performance in converting biomechanical energy, such as heartbeat, respiratory motion, limb movements and pulse pulsation.<sup>[21–26]</sup> The converted electrical energy were succeeded in cardiac pacemaker, health monitoring, cell and tissue engineering.<sup>[26–31]</sup> Zheng et al. have reported the first fully biodegradable TENG consisted of artificial synthetic polymers (poly(lactic-co-glycolic acid) (PLGA), poly(3-hydroxybutyrate-co-3-hydroxyvalerate) (PHBV), and polycaprolactone (PCL)) in 2016,<sup>[31]</sup> which can be purchased from companies. However, these commercial polymers usually have a high price and contain potentially harmful chemicals. Compared with these synthetic polymers, natural polymers received increasing attention for their low cost, easy availability, renewability, and good biocompatibility.<sup>[32–35]</sup> These features endow them with wide application in biomedical fields, such as drug delivery, absorbable suture, and vascular scaffold.<sup>[36–41]</sup> These natural bioresorbable polymers (NBP) mainly include cellulose, chitin, silk fibroin (SF), rice paper (RP), egg white (EW), and so on. These materials possess advantages of excellent biodegradability, easy processability, and good film-forming property, which make them suitable for TENG components for in vivo applications.

Herein, using the abovementioned natural biodegradable materials, various fully bioresorbable natural-materials-based TENGs (BN-TENGs) were developed. Compared with previous reported TENGs,<sup>[31–35]</sup> this work first fabricated fully in vivo absorbable BN-TENGs using five natural materials. A comprehensive research of “triboelectric series” of these materials was first conducted by pairwise combinations test, which greatly promoted the development of natural materials applied in TENG and other triboelectric devices. The operation time of BN-TENG in vitro and in vivo was tuned by encapsulation of silk fibroin film from days to weeks. Using the proposed BN-TENG as a voltage source to power an electrical stimulation system in vitro, the function of isolated dysfunctional cardiomyocyte clusters was successfully regulated. The beating rates of cardiomyocyte clusters were accelerated, and the consistency of contraction was improved. The therapeutic efficacy of BN-TENG on dysfunctional cardiomyocytes provided a new and valid solution to treat some heart diseases, such as bradycardia and arrhythmia. After completing its function, the BN-TENG can be fully degraded and resorbed in Sprague–Dawley (SD) rats. Considering its controllability, bioabsorbability, low cost, and easy availability, this proposed BN-TENG has a great application potential as a bioabsorbable power source for future transient electronics and IMDs.

As shown in **Figure 1a**, all the polymeric components of BN-TENGs originated from nature, including cellulose, chitin, RP, SF, and EW. Cellulose can be prepared from wood and cotton; chitin can be extracted from shells of crab and shrimp; RP usually comes from wheat, corn, and rice; and EW and SF can be collected from egg and cocoon, respectively. The as-prepared BN-TENG consisted of NBPs and magnesium (Mg) electrodes with a vertical contact-separation mode (**Figure 1b**). Any two different NBPs (NBP1 and NBP2) from chitin, cellulose, SF,

RP, and EW could act as friction layers, and the ultrathin Mg films served as the back electrodes. The friction surface of NBPs was treated with inductively coupled plasma-reactive ion etching (ICP) to form nanostructure arrays to enlarge the effective contact area and enhance the contact electrification. The obtained nanostructure arrays were dense and homogeneous, with an average height of about 100 nm (**Figure 1c,d**). Two NBP spacers were placed between the friction layers to separate them effectively. The SF films served as encapsulation layers to protect BN-TENG from external environment (**Figure 1b**).

When we chose SF and RP as the friction layers for an example, the fabricated BN-TENG showed the maximum output voltage and current values of 34 V and 0.32  $\mu\text{A}$ , respectively (**Figure 1e,f**). When the measurement instrument was reversely connected to BN-TENG, the output voltage and current signals were correspondingly inversed, which indicated that the signals were generated by the BN-TENG (**Figure 1g,h**). The effective output power of the BN-TENG was evaluated by monitoring the voltage and current with variable load resistances ranging from 1 k $\Omega$  to 1 G $\Omega$  (**Figure 1i**). The current amplitude decreased with the increasing of load resistance due to the ohmic loss, while the voltage followed a reverse trend, and an optimized power density of 21.6 mW m<sup>-2</sup> was achieved with a load resistance of about 67 M $\Omega$  (**Figure 1j**). The inset in **Figure 1j** demonstrated that ten commercial green LEDs can be instantaneously lit up by the BN-TENG. These LEDs were directly powered by pressing and releasing the BN-TENG without external power supply. It showed that the as-fabricated BN-TENG can convert ambient mechanical energy into electrical energy effectively and power other electronic devices.

Biocompatibility is one of the essential requirements for implantable devices, which largely depends on the encapsulation strategy and component materials. In this paper, five NBPs were processed into thin films and evaluated the biocompatibility by L929 cells. These NBPs were prepared to thin films of 1 cm  $\times$  2 cm in size and 100  $\mu\text{m}$  in thickness, which showed an excellent film-forming ability. All these films possessed a certain degree of transparency and flexibility (**Figure 2a** and **Figure S1**, Supporting Information). The relatively rough surfaces of the NBP films also contributed to cell attachment and proliferation on their surface (**Figure S2**, Supporting Information). The viability of L929 cells on five films were studied by 3-(4,5-dimethylthiazol-2-yl)-2,5-diphenyltetrazolium bromide (MTT) assay (**Figure 2b**). The optical density values of the control groups at 1, 2, and 3 d were set as 1 and selected as the reference value for other corresponding experimental groups. After incubation for 1 d, the relative viabilities of L929 cells on five films were all higher than 95%. After incubation for 2 and 3 d, the relative viabilities of L929 cells on five films were all higher than 96%. Statistical results also showed in **Figure 2b**. These results demonstrated that the L929 cells cultured on these films can grow and proliferate without obvious stagnation, which proved that these five NBPs had nontoxic essentially.

To further investigate the attachment, proliferation and morphology of L929 cells on these NBP films, immunofluorescence staining was carried out at 1, 2, and 3 d, respectively (**Figure 2c**). After culturing for 24 h, L929 cells with a low density showed good attachment and cellular morphology as single cells (1 d in **Figure 2c**). After incubation for 2 and 3 d, the L929 cells obviously reached high cellular density and showed a good

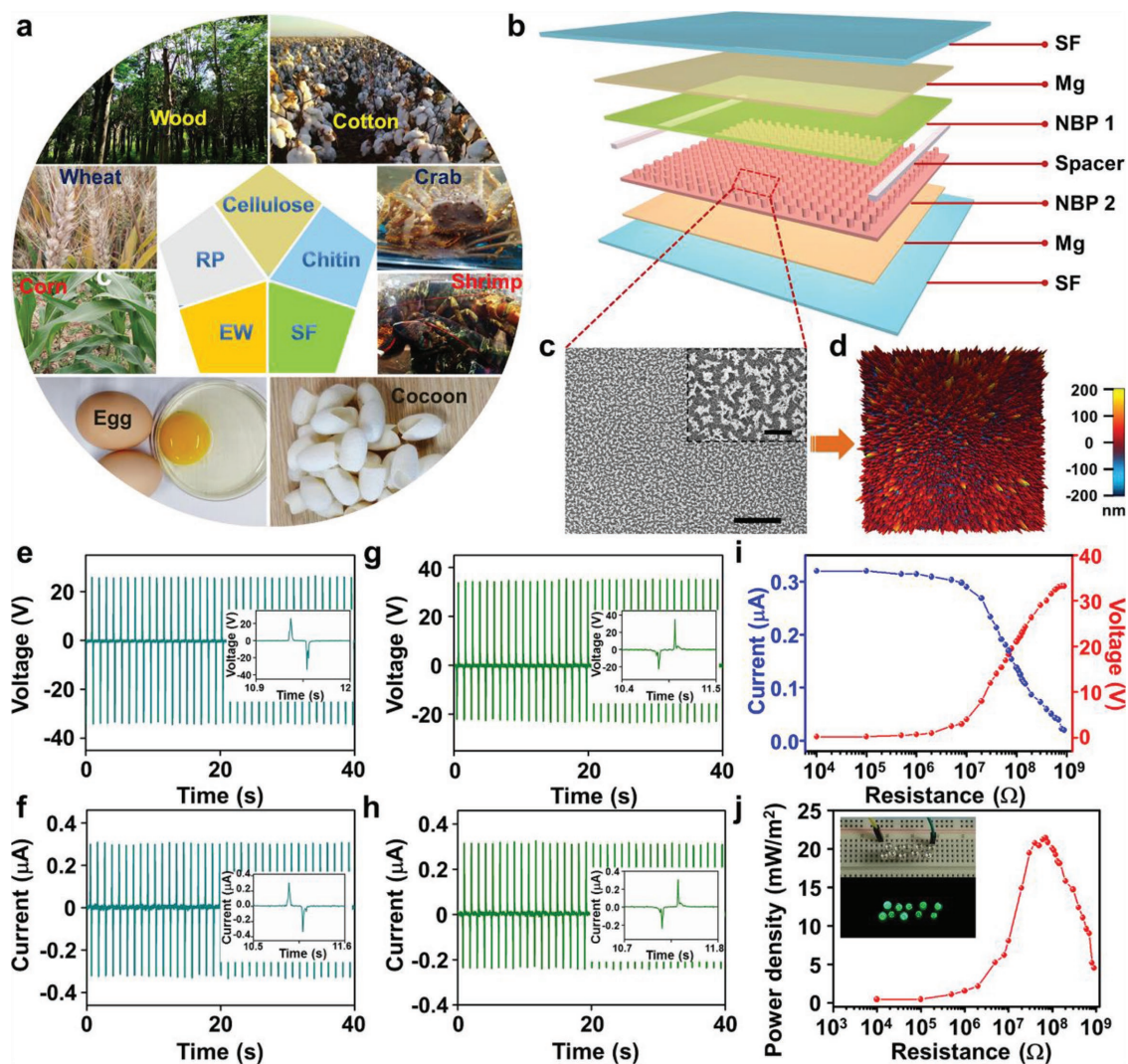


**Figure 1.** a) NBPs originating from nature with wide raw material sources. b) Structure diagram of a typical BN-TENG device. c,d) Scanning electron microscopy (SEM) and atomic force microscopy (AFM) images of nanostructure on the surface of NBP film. Lower and upper scale bars: 5 and 1  $\mu\text{m}$ . e–h) Output voltage and current of BN-TENG measured with forward connection (e,f) and reverse connection (g,h). i) The dependence of output voltage and current on the external loading resistance. j) The dependence of the power density on the external loading resistance. The inset shows photographs of ten commercial LEDs before and after lit by a BN-TENG.

filamentous, stretched morphology (2 and 3 d in Figure 2c). Some cell clusters appeared and even formed a confluent cell monolayer (3 d in Figure 2c). The results coincided with those of MTT assay, which indicated that L929 cells showed good attachment, spreading, and growth on these films. It demonstrated that the five NBPs are biocompatible and nontoxic, which can guarantee the biosecurity of the implanted BN-TENG.

The as-fabricated BN-TENG (Figures S3 and S4, Supporting Information) converted mechanical energy to electricity with a contact and separation mode. The coupling of triboelectric effect and electrostatic induction between friction layers generates an alternating flow of electrons between two back electrodes.<sup>[42,43]</sup> As shown in Figure 3a, when an external force brought the friction layers into physical contact between top and bottom surfaces, oppositely charged surfaces were created for the different electron affinity of NBPs (original and pressed in Figure 3a). Once the external force disappeared,

the friction layers were separated by the spacers and a potential drop between the back electrodes impelled the free electrons transferred from one electrode to the other electrode to balance the electrostatic field (releasing in Figure 3a). When the gap increased from minimum to maximum, the potential drop stemmed from triboelectric charges disappeared gradually (released in Figure 3a). When the external force brought the friction layers into contact again, the induced electrons will flow back and created a reverse current (pressing in Figure 3a). The periodic contact and separation of friction layers resulted in an AC output signal in the external circuit.

In order to quantify the electrical output performance of BN-TENG, the “triboelectric series” of the five NBP films were ranked basing on their abilities of gaining or losing electrons.<sup>[44,45]</sup> A Kapton film was selected as the reference friction layer of TENG in all pairwise combinations. The quantity of transferred charges between the NBP films and Kapton film were recorded



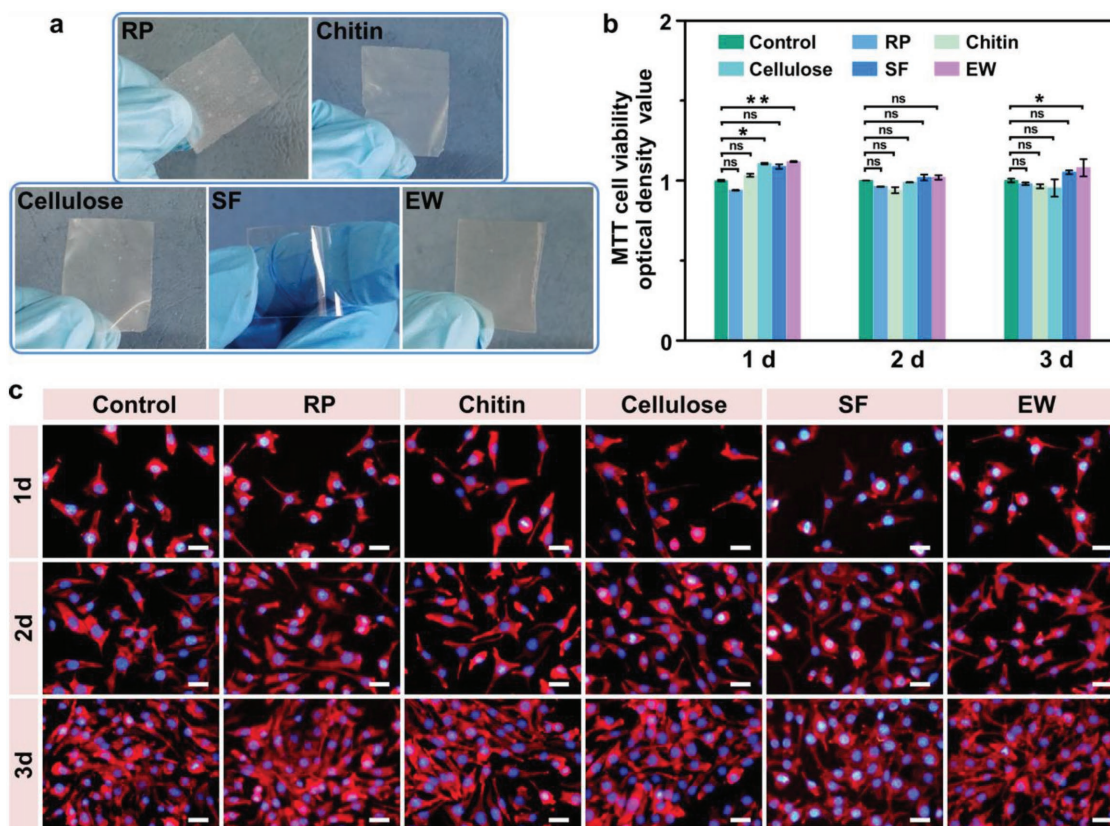


**Figure 2.** a) Film pictures of RP, chitin, cellulose, SF, and EW. b) MTT assays of L929 cells cultured on NBP films for 3 d. All the data are presented as the means  $\pm$  SD. *P*-values are calculated by *t*-test. \**P* < 0.05, \*\**P* < 0.01, NS = nonsignificant. c) Immunofluorescent staining of L929 cells cultured on NBP films. Scale bar: 50  $\mu$ m.

in Figure 3b. The pair combination of EW and Kapton showed the maximum transferred charges (12 nC), RP and Kapton presented the minimum transferred charges (5.5 nC). According to the difference in transferred charges, the triboelectric series of the five NBP films was defined as EW > SF > chitin > cellulose > RP from positive to negative (Figure 3b). Then various BN-TENGs were assembled basing on the triboelectric series above. With different pairwise combinations, the as-fabricated BN-TENG achieved a wide range of tunable output performance for  $V_{oc}$  from 8 to 55 V and  $I_{sc}$  from 0.08 to 0.6  $\mu$ A (Figure 3c and Figure S5, Supporting Information). The low current can be attributed to the small size (1 cm  $\times$  2 cm) of BN-TENG and low beating frequency of linear motor.<sup>[46,47]</sup> These results indicated that the BN-TENG can satisfy a wide range of electrical output requirements, such as different voltages for bioelectric stimulation or powering different energy consumption devices.

According to previous reports, methanol can transform the molecular structure of SF from random coil into  $\beta$ -sheet conformation, which contributes to strengthening the resistance of BN-TENG to phosphate buffered saline (PBS) and body fluid.<sup>[48–50]</sup> To achieve a controllable operation time of BN-TENG in SD rats, untreated SF (U-SF) and methanol treated SF (M-SF) films were prepared as encapsulation layers, respectively, for BN-TENGs (Figure S6, Supporting Information). The biodegradability and bioabsorbability of the BN-TENGs were studied *in vitro* (Figure 4a,c) and *in vivo* (Figure 4b,d).

As shown in Figure 4a,c, the BN-TENGs encapsulated with U-SF and M-SF films kept structural integrity in PBS at 1 d. After 7 d, the integral structure of U-SF encapsulated BN-TENG swelled and wrinkled due to the fracture of polymer backbone. Mg electrodes were totally corroded by PBS due to water infiltration. After 21 d, about one fourth of the BN-TENG disappeared due to structural cracking. When the BN-TENG was immersed in PBS for a longer time, rapid autocatalytic hydrolysis and bulk degradation happened (42 d), and the integral structure degraded and dissolved into PBS (84 d). By comparison, the degradation rate of M-SF encapsulated BN-TENG was much slower in PBS. It kept structure integrity until 42 d. An obvious shape deformation formed after 84 d. These results indicated that M-SF films can significantly protect the BN-TENG from hydrolysis and inhibit its degradation in PBS.

As shown in Figure 4b,d, both U-SF and M-SF encapsulated BN-TENGs *in vivo* kept structural integrity at 1 d. The U-SF encapsulated BN-TENG swelled and wrinkled under the fracture of polymer backbone. Some gaps formed at the edges of BN-TENG at 7 d. After 21 d, the U-SF encapsulated BN-TENG *in vivo* was disintegrated into two parts, which can be attributed to the impact of the metabolism of the SD rat, the surrounding fibrous tissue around the BN-TENG and the daily running of SD rat itself. After 42 and 84 d, the cracked parts of BN-TENG degraded and absorbed by the SD rat. By comparison, the degradation rate of M-SF encapsulated BN-TENG in

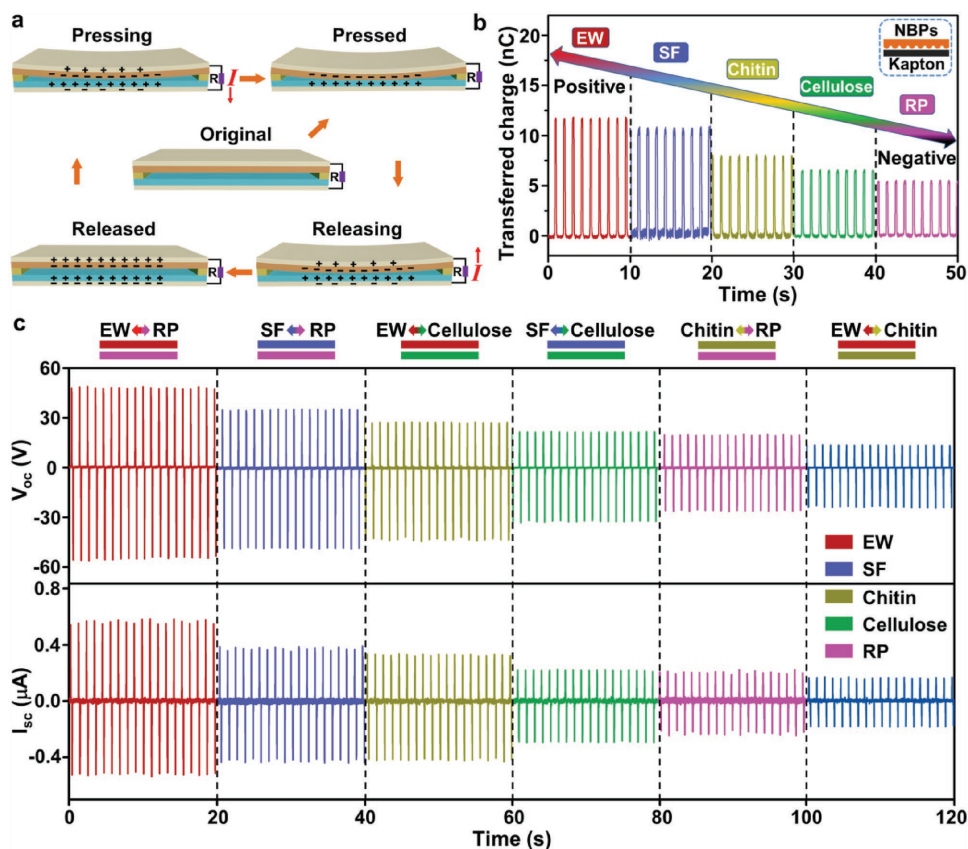


**Figure 3.** a) Schematic diagram that illustrates the working principle of BN-TENG with the vertical contact-separation mode. b) Relative ability ranking of gaining or losing electrons of five NBP films. The Kapton film served as the reference friction layer in all pairwise combinations. c) The output performances of BN-TENGs with different pairwise combinations. Above: open-circuit voltage ( $V_{oc}$ ). Below: short-circuit current ( $I_{sc}$ ).

vivo was much slower. It kept structural integrity until 42 d. An obvious shape deformation formed until 84 d, which showed that the M-SF films can also slow down the degradation rate of BN-TENG effectively in vivo. All the results above proved that the BN-TENG has a good biodegradability in vitro and in vivo. The degradation rate of BN-TENG in vitro and in vivo can be controlled effectively by modifying SF encapsulation layers, which provided a guidance to design the implantable BN-TENG for short-term and long-term applications. Additionally, considering the practical application in future, the flexibility and robustness of the whole device could be further improved by new material selection, structure design or chemical/physical modification to enhance the resistance of BN-TENG to biological environment.

For proving the as-fabricated BN-TENGs were capable of converting biomechanical energy to electrical energy in a living body, BN-TENGs (SF/RP) encapsulated with U-SF and M-SF films were implanted in the dorsal subcutaneous region of SD rats (Figure 5a and Figure S7, Supporting Information). All the implantation operations were performed strictly in accordance to “Beijing Administration Rule of Laboratory Animals” and the national standard “Laboratory Animal Requirements of Environment and Housing Facilities (GB 14925-2001).” The wound was instantly sutured after implantation. After 8 weeks, the wound healed well and showed no obvious infection and inflammation. The in vivo electrical output performance of

the BN-TENGs was measured at different time. As shown in Figure 5b–d, an M-SF encapsulated BN-TENG was implanted in dorsal subcutaneous region of an SD rat. The SD rat was performed euthanasia after 13 weeks, and its subcutaneous tissue containing residual BN-TENG at the implantation site was taken for histological study. The hematoxylin and eosin (H&E) stained histologic section showed that some residues (blue arrow) of BN-TENG existed between the subcutaneous layer and the muscle layer (Figure 5e). The residues were surrounded by small amounts of fibrous tissue and macrophages. Some regenerated normal tissues containing macrophages (green arrow) formed in the gaps between residues. No neutrophil granulocyte and obvious inflammation were observed, revealing good in vivo biocompatibility and bioabsorbability of the BN-TENG.

The electrical outputs of the BN-TENGs were recorded throughout the in vivo implantation (Figure 5f,h,i). As for M-SF encapsulated BN-TENG, the output voltage decreased from 4.5 to 1.2 V at 11 d. It can be ascribed to the constraint of the surrounding fibrous capsule around the BN-TENG, the swelling wrinkles of encapsulation layer and the decline of mechanical property of friction layers (Figure 5f,h). Although the swelling encapsulation layer would restrict the contact and separation of BN-TENG, no body fluid permeation occurred between the friction layers. The output performance of BN-TENG was weakened with the time of implantation. The electrode wires fell off

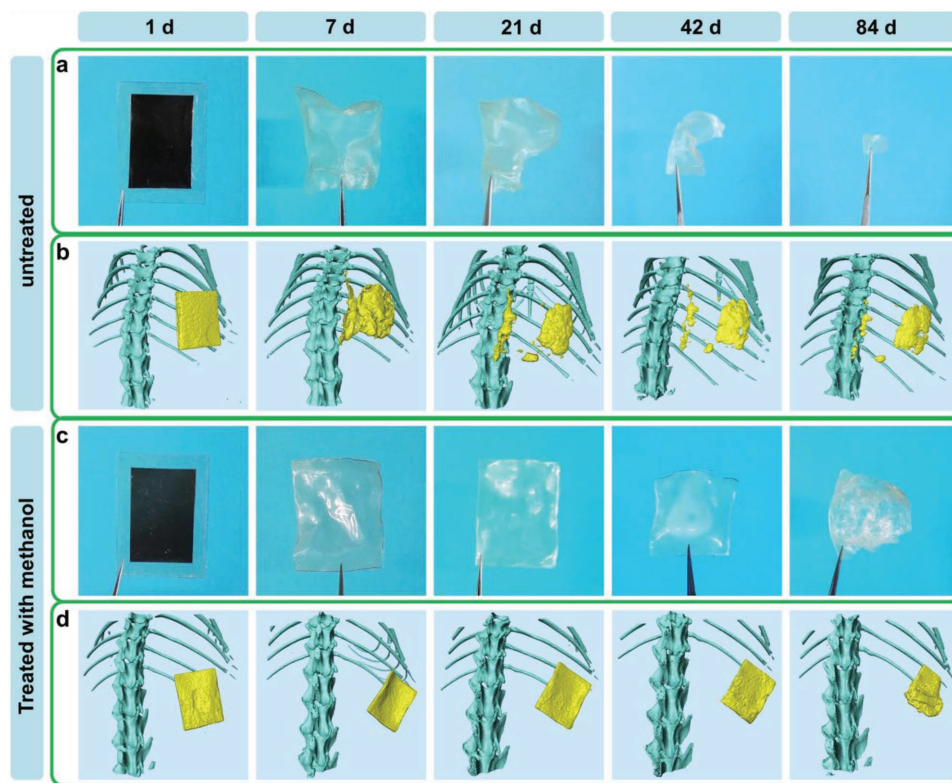


**Figure 4.** a,c) In vitro biodegradation simulation of BN-TENG encapsulated with U-SF films (a) and M-SF films (c) in PBS at 37 °C. b,d) In vivo biodegradation of BN-TENG encapsulated with U-SF films (b) and M-SF films (d) in SD rats. All the images in (b) and (d) were reconstructed from a micro-CT system and processed with pseudocolor technology.

from Mg back electrodes after 4 weeks, indicating that the body fluid had permeated into the encapsulation layers and corroded back electrodes of Mg. Compared with U-SF films, the M-SF films can not only keep a relatively good structural integrity, but also a slow mass loss for a relatively long time (Figure 5g). This feature made M-SF encapsulated BN-TENG achieve a long-term operation time.

The electrical output performance of the U-SF encapsulated BN-TENG was also evaluated with a short-term operation time (Figure 5f,i). Compared with the M-SF encapsulated BN-TENG, the U-SF encapsulated BN-TENG exhibited a rapid degradation behavior. The in vivo output voltage decreased rapidly from 3 to 0.6 V within 24 h (Figure 5f,i). After 72 h, the in vivo electrical output was completely destroyed. The reason is probably that with the hydrolysis of encapsulation layer, the triboelectric effect of BN-TENG was damaged due to the body fluid permeation. The in vitro biodegradation test also showed a rapid mass loss for U-SF encapsulated BN-TENG (Figure 5g). Only 37.5% of the initial mass was remained at 7 d because of the fast dissolution and hydrolysis of U-SF layers and Mg electrodes. This resulted in the destruction of structural integrity and significant electrical output loss of BN-TENG in a short time.

The results above demonstrated that the BN-TENG has good biocompatibility and bioabsorbability. The as-fabricated BN-TENG can effectively convert biomechanical energy to electrical energy in vivo with a controllable operation time. The operation time of BN-TENG can be effectively modulated by modifying the SF encapsulation layers for long-term and

short-term applications. After finishing its work, the BN-TENG can be degraded and resorbed by SD rats.

The electrical stimulation in tissue engineering offers a promising route for cell regulation and tissue repairing. A variety of researches proved its feasibility and effectiveness in clinical and research settings.<sup>[51–53]</sup> Herein, the electrical output of BN-TENG featured relative high voltage and low current, which were propitious to the electric stimulation in a biomedical field. In order to demonstrate the practicability of utilizing BN-TENG for regulating the beatings of cardiomyocyte clusters, the as-fabricated BN-TENG and interdigital electrode were integrated into a self-powered stimulation system. As shown in Figure 6a, the stimulation system consisted of a BN-TENG, a rectifier and a microgapped interdigital electrode. The interdigital electrode was packaged with a thin poly(dimethylsiloxane) (PDMS) film of 50  $\mu\text{m}$  thick to avoid electrochemical reaction between electrodes and culture medium (Figure 6c). The rectified output voltage of 18 V produced by BN-TENG was connected to the interdigital electrodes to form a DC electric field (Figure 6a,b). Considering the thickness of the PDMS package layer, the actual electric field (EF) strength at the interface between the cardiomyocytes and device was about 8  $\text{V cm}^{-1}$ , which was calculated by finite element simulation (Figure S8, Supporting Information).

Then the primary cardiomyocytes were seeded on the surface of the interdigital electrodes. According to previous report, the cardiomyocytes can generate electrical interconnections via gap junction proteins (i.e., connexin) that mediate intercellular communication.<sup>[49–52]</sup> During the incubation, the seeded



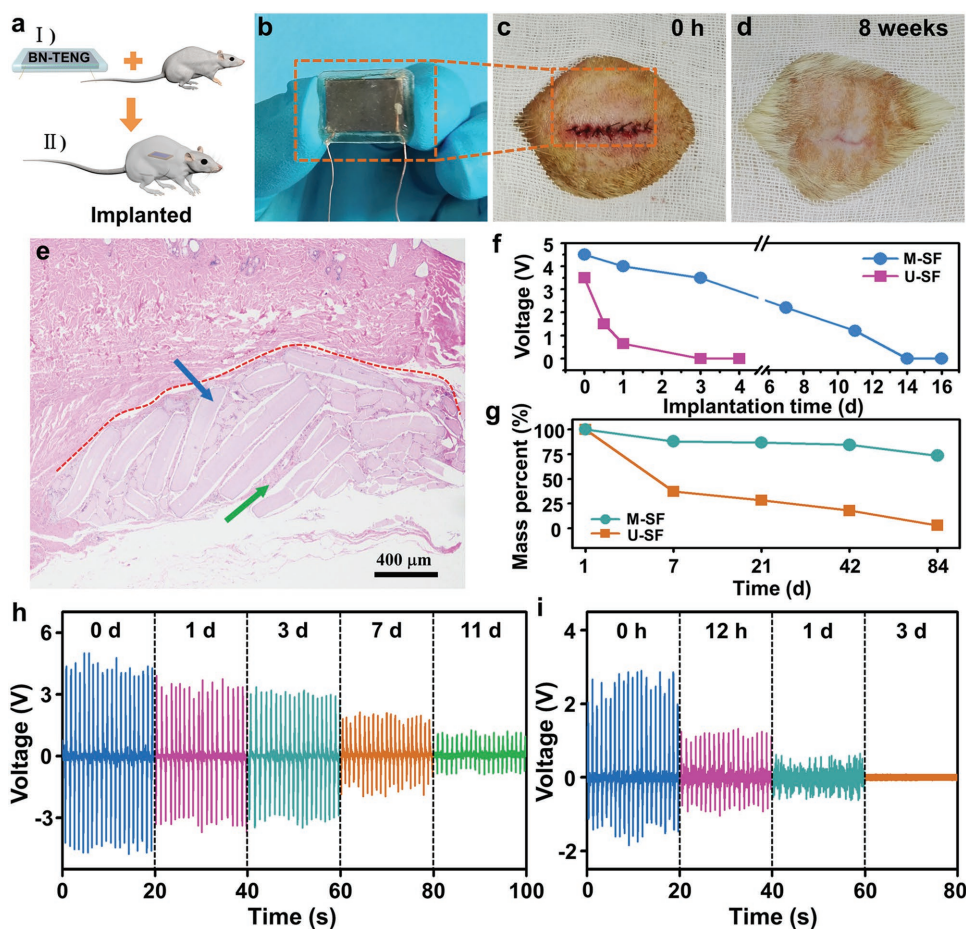


**Figure 5.** a) Implantation schematic of the BN-TENG. b) Picture of an M-SF encapsulated BN-TENG. c) Initial state of the implantation site after suture. d) Recovery of implantation site after 8 weeks. e) H&E stained histologic section at the implantation site of the SD rat. The red dashed line marks the boundary between BN-TENG residues and subcutaneous tissue. The blue arrow indicates the degradation residues of the BN-TENG. The green arrow indicates the regenerated normal tissue containing macrophages around the BN-TENG residues. f) In vivo output voltage of U-SF and M-SF encapsulated BN-TENGs in SD rats. g) In vitro mass variation of U-SF and M-SF encapsulated BN-TENG as a function of immersion time in PBS at 37 °C. h,i) In vivo electrical output of M-SF and U-SF encapsulated BN-TENG at different implantation time, respectively.

cardiomyocytes interconnected with each other and formed isolated cardiomyocyte clusters in electrode gap (Figure 6d). After incubation for 48 h, the cardiomyocyte clusters (C1, C2, C3, and C4 in Figure 6d) beat slowly with a long pause (Video S1, Supporting Information) before the electrical stimulation. The contraction of cardiomyocytes in clusters is weak and inactive, especially the cardiomyocytes in C2 and C3. Then, the cardiomyocyte clusters were continuously stimulated for 30 min at 1 Hz with the DC-EF from BN-TENG.

After electrical stimulation with the BN-TENG, the beating rates of the four cardiomyocyte clusters accelerated significantly. The cardiomyocytes in clusters become more vigorous (Video S1, Supporting Information). Specifically, taking cardiomyocyte cluster in C1 as the example, the average pause time between two beating cycles of the cardiomyocyte cluster was greatly reduced from 1.382 to 0.606 s after stimulation (Figure 6e). Furthermore, the average contraction time in one cycle was also reduced from 0.320 to 0.240 s in C1 (Figure 6f). The beating rate of the cardiomyocyte cluster increased significantly after the stimulation. Figure 6g summarized the

beating rates of the four cardiomyocyte clusters before and after the stimulation by DC-EF from BN-TENG. It showed that the beating rates of the four clusters increased tremendously after the stimulation, especially for C2 and C3. The beating rates of cardiomyocyte clusters in C2 and C3 increased by about 8.8 times.

Moreover, according to the statistical results, reflecting dispersion of these cardiomyocyte clusters before and after the stimulation (Table S1, Supporting Information), the coefficient of variation before the stimulation was 0.81, which was about 2.6 times that after the stimulation. This means that the variation of beating rates of the four cardiomyocyte clusters decreased significantly after the stimulation by DC-EF from BN-TENG. The beating rates tend to be more uniform between each cardiomyocyte cluster and keep consistent after the EF stimulation. The reason was probably that the electrical stimulation enhanced the intercellular communication and reestablished the contractile function of the dysfunctional cardiomyocyte clusters, which was supported by previous literatures.<sup>[51–54]</sup> This BN-TENG integrated self-powered stimulation system can

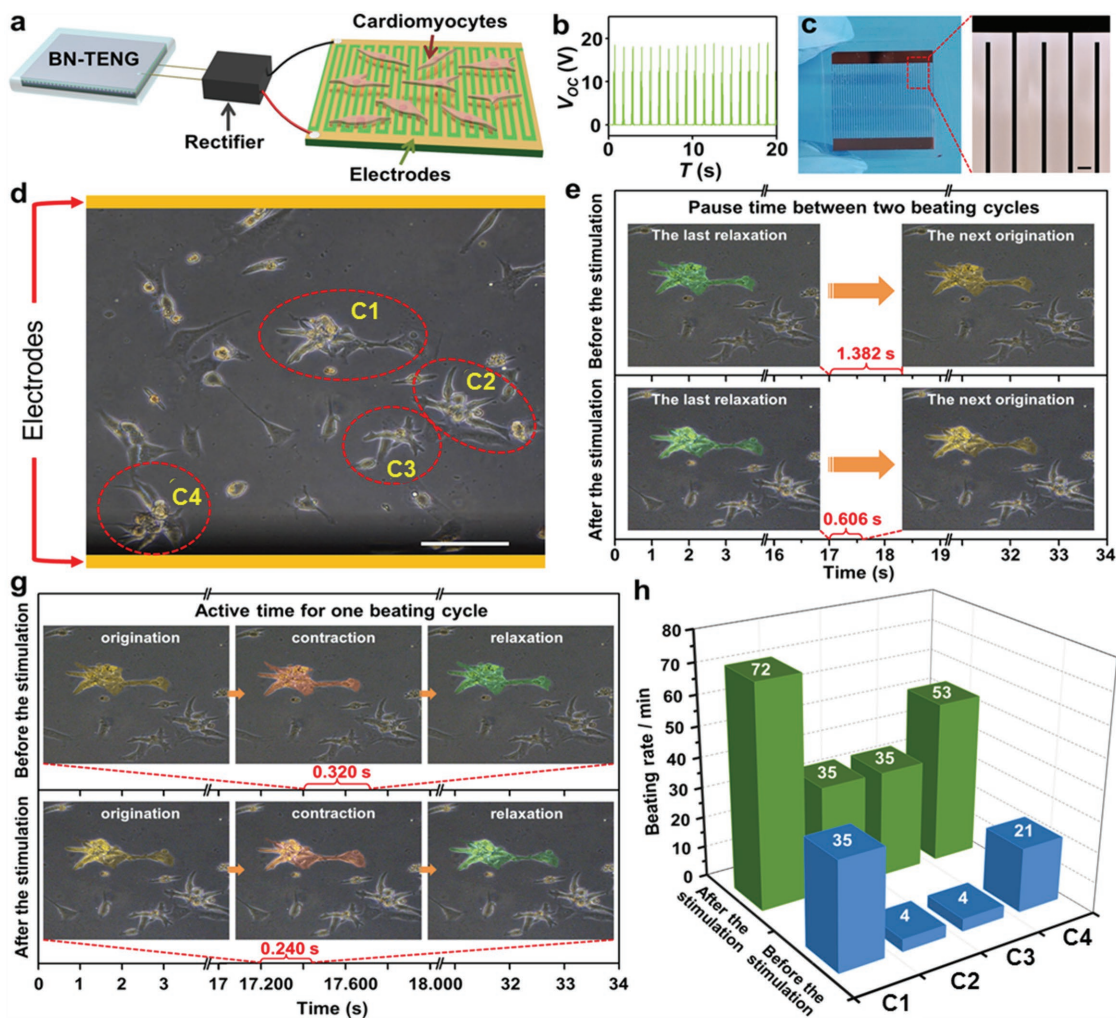


**Figure 6.** a) Schematic diagram of the stimulation system. b) Rectified electrical output of BN-TENG. c) Optical image (left) and magnified image (right) of the interdigital electrode. Scale bar: 300  $\mu\text{m}$ . d) Microscopy image of cardiomyocytes cultured on the surface of the interdigital electrode. The red circles (C1, C2, C3, and C4) represent four different cardiomyocyte clusters. e) Pause time between two adjacent beating cycles of cardiomyocyte cluster in C1 before and after the stimulation. f) Active time for one beating cycle of cardiomyocyte cluster in C1 before and after the stimulation. g) Beating rates of the four cardiomyocyte clusters (C1, C2, C3, and C4) before and after the stimulation. The beating rate refers to the beating times of cardiomyocyte cluster in one minute.

be directly utilized to coordinate and repair the abnormal cardiomyocytes. It may provide a new and valid solution to treat some heart diseases, such as bradycardia and arrhythmia. It is also potentially used for rebuilding myocardial tissues in vivo.

In summary, we developed fully bioabsorbable BN-TENGs in vivo using five natural materials, including chitin, cellulose, SF, RP, and EW. The “triboelectric series” of these materials was ranked for the first time, that is, EW > SF > Chitin > Cellulose > RP from positive to negative. It provided a basic knowledge for TENG design using natural materials. The operation time of BN-TENGs in vivo and in vitro was modulated from days to weeks by modification of SF encapsulation film. A wide range of electric output of BN-TENGs was generated for  $V_{oc}$  from 8 to 55 V and  $I_{sc}$  from 0.08 to 0.6  $\mu\text{A}$ , respectively. Using the BN-TENG as a power source, the beating rates of dysfunctional cardiomyocyte clusters were accelerated, the

consistency of cell contraction was improved, which provided a new and valid solution to treat some heart diseases, such as bradycardia and arrhythmia. After completing its function, the proposed BN-TENG can be fully degraded and absorbed in SD rats. Allowing for its impressing in vitro and in vivo electrical output, good biocompatibility, tunable biodegradability and bioabsorbability, the BN-TENG proposed in this work has a great potential as a power source for transient electronics, and bioresorbable IMDs in the future.

## Experimental Section

**Preparation of SF Film:** Raw silk was immersed in  $\text{Na}_2\text{CO}_3$  aqueous solution, boiled for 30 min, and thoroughly rinsed with substantial deionized (DI) water. The obtained degummed silk (6.5 wt%) was dissolved in the  $\text{CaCl}_2$ /ethanol aqueous solution system with vigorous



stirring at 78 °C. Subsequently, the obtained homogeneous solution was filtered with a millipore filter (0.22 μm), dialyzed against DI water using a dialysis tubing (3.5k molecular-weight cut-off (MWCO)), and further freeze dried for 48 h to obtain pure solid SF. Then, a certain amount of the solid SF was dissolved in hexafluoroisopropanol (HFIP) solution (1 g mL<sup>-1</sup>). Some of the as-prepared solution was added into a teflon flat dish, put in a fume cupboard, and air dried at room temperature for 12 h.

**Preparation of RP Film:** The rice paper was purchased and used directly without further treatment.

**Preparation of EW Film:** Egg-white solution was coated on an SF membrane substrate and then heated at 60 °C, until solidification.

**Preparation of Chitin Film:** The purified chitin powders (6 wt%) were dispersed into the NaOH/urea aqueous solution. After frozen treatment, the mixture was vigorously stirred to form a homogeneous solution. The obtained solution was centrifuged to eliminate bubbles, coated on a glass plate, and then immersed into ethanol solution. The obtained chitin gel was thoroughly rinsed with substantial DI water and air dried at room temperature for 24 h.

**Preparation of Cellulose Film:** The cellulose fibers (5 wt%) were added into the NaOH/urea aqueous solution system. After frozen treatment, the mixture was vigorously stirred to form a homogeneous solution. The obtained solution was centrifuged to eliminate bubbles, coated on a glass plate, and then immersed into ethanol solution. The obtained cellulose gel was thoroughly rinsed with substantial DI water and air-dried at room temperature for 24 h.

**Fabrication of BN-TENG Based on SF and RP Films:** The as-prepared SF film was treated with ICP technology to obtain the nanostructures on its surface. Then the flat surface of SF film was sputtered with a thin magnesium (General Research Institute of Nonferrous Metals, Beijing, China) layer as the back electrode. The RP film was also sputtered with the back electrode. Then the two films were assembled together with two spacers between them. Finally, two lead wires were connected to the back electrodes, respectively. BN-TENGs with other pairwise NBP combinations shared the same fabrication method.

**Cell Culture:** The as-prepared films above were fixed on the surface of glass slices, sterilized and placed into a 24-well culture plate. The L929 cells (1 × 10<sup>4</sup> cells well<sup>-1</sup>) were seeded on the surfaces of these films and cultured in Dulbecco's modified Eagle medium (DMEM) containing 10% fetal bovine serum, 100 U mL<sup>-1</sup> penicillin, and 100 μg mL<sup>-1</sup> streptomycin. The L929 cells were incubated in a cell incubator with a humidity atmosphere containing 5% CO<sub>2</sub> at 37 °C for 24, 48, and 72 h, respectively.

**MTT Assay:** Cell viability and proliferation were assessed by MTT assay. Briefly, 100 μL of MTT assay solution (5 mg mL<sup>-1</sup>) was added into each well, and the cells were kept still for 4 h at 37 °C. After removing the supernatant, 200 μL of dimethyl sulfoxide was used to dissolve the generated MTT formazan for 2 h at room temperature. Optical densities were characterized at 570 nm using a spectrophotometer (BioTek, Synergy HTX).

**Fluorescence Staining:** The cellular F-actin cytoskeleton and nucleus were stained with red-fluorescent Alexa Fluor 594 phalloidin and blue-fluorescent 4',6-diamidino-2-phenylindole (DAPI), respectively. The cultured L929 cells were stained following a standard protocol. Briefly, cells were washed with PBS for three times, fixed with paraformaldehyde (4%) in PBS for 15 min at room temperature, permeabilized with 0.1% TritonX-100 in PBS, and further incubated with 1% bovine serum albumin in PBS. Subsequently, Phalloidin and DAPI stain solutions were successively added. Finally, the stained cells were characterized using a confocal laser scanning microscope (Leica, SP8).

**Fabrication Process of SF Layers Used in In Vivo Degradation for Microcomputed Tomography (CT) Imaging:** BaSO<sub>4</sub> nanoparticles were utilized as the radiopaque contrast medium in X-ray micro-CT imaging and uniformly distributed into SF films to form the BaSO<sub>4</sub>/SF composite films. In detail, the BaSO<sub>4</sub> nanoparticles (4 wt%) were added in the SF HFIP solution, and then treated with ultrasonication for 10 min. The obtained mixed solution was added into a teflon flat dish and air dried at room temperature for 12 h.

**Fabrication Process of M-SF Films:** One surface of the SF film was sprayed with anhydrous methanol for four times. The interval time of

adjacent sprayings was 2 min. The as-prepared films were defined as M-SF films. The SF films that were not treated with anhydrous methanol were defined as U-SF films. The as-prepared SF films with an M-SF surface and a U-SF surface were used as the encapsulation layers for BN-TENG.

**In Vitro Electrical Measurement of BN-TENG:** The electrical properties of BN-TENG were mechanically measured with a liner motor system that applied a periodical compressive force at a frequency of 1 Hz. The resulting applied strain on the BN-TENG was about 0.06% by calculation. The output V<sub>oc</sub> was characterized with a digital oscilloscope (Teledyne LeCroy, HDO6104). The output I<sub>sc</sub> and the quantity of transferred charges were both measured by using an electrometer (Keithley, 6517B).

**In Vivo Implantation and Electrical Measurement of BN-TENG:** Before the implantation operation, the BN-TENGs and all surgical instruments were sterilized by <sup>60</sup>Co-Gamma-ray irradiation and autoclaving methods. The SD rats were anaesthetized with the intraperitoneal injection of pentobarbital sodium (30 mg kg<sup>-1</sup>). The as-sterilized BN-TENGs were implanted into the subcutaneous region of the SD rats. When electrical signals were measured, an external force by a slight finger tap was performed on the skin of the implantation site to drive the implanted BN-TENG. The output performance was characterized with a digital oscilloscope.

**Fabrication of Electric Stimulation System:** Au interdigital electrodes were prepared on the quartz glass substrate by photolithography and magnetron sputtering methods. The space between two adjacent electrodes was 500 μm. The BN-TENG was connected to the interdigital electrodes using a rectifier bridge. The as-prepared interdigital electrodes were then encapsulated with a thin PDMS film to isolate itself from the culture medium.

**Stimulation of Cardiomyocyte Clusters:** The stimulation system was sterilized and placed into a petri dish. The primary cardiomyocytes were extracted from neonatal SD rats (1–3 d old) and seeded on the surface of the stimulation device. The culture medium consisted of DMEM containing 10% fetal bovine serum, 100 U mL<sup>-1</sup> penicillin, and 100 μg mL<sup>-1</sup> streptomycin. The cardiomyocytes were incubated in an incubator with a humidity atmosphere containing 5% CO<sub>2</sub> at 37 °C for 48 h. The rectified EF of BN-TENG was applied on the cultured cardiomyocytes for 30 min. The beating rates of the cardiomyocytes were recorded by an inverted phase contrast microscope with a charge coupled device camera system before and after the electrical stimulation.

**Statistical Analysis:** The data were present as the mean ± SD (standard deviation), with a group size: n ≥ 3. A two-tailed unpaired t-test was used to calculate the P-values. Statistical significance was accepted at \*P < 0.05, \*\*P < 0.01, \*\*\*P < 0.001.

## Supporting Information

Supporting Information is available from the Wiley Online Library or from the author.

## Acknowledgements

W.J., H.L., and Z.L. contributed equally in this work. This work was supported by the national key R&D project from Minister of Science and Technology, China (2016YFA0202702, 2016YFA0202703), National Natural Science Foundation of China (31571006, 81601629, and 61501039), Beijing Talents Fund (2015000021223ZK21), the Beijing Natural Science Foundation (2182091 and 2162017), and “Thousands Talents” program for pioneer researcher and his innovation team.

## Conflict of Interest

The authors declare no conflict of interest.

## Keywords

bioabsorbable, biodegradable, natural materials, transient electronics, triboelectric nanogenerators

Received: March 25, 2018

Published online:

- [1] K. Bazaka, M. Jacob, *Electronics* **2013**, 2, 1.
- [2] W. H. Maisel, *JAMA* **2005**, 294, 955.
- [3] D. Kim, H. Shin, H. Park, G. Hwang, D. J. Joe, J. Han, B. Joung, K. Lee, *Adv. Funct. Mater.* **2017**, 27, 1700341.
- [4] J. A. Rogers, *JAMA* **2015**, 313, 561.
- [5] S. J. A. Majerus, S. L. Garverick, M. A. Suster, P. C. Fletter, M. S. Damaser, *J. Emerg. Technol. Comput. Syst.* **2012**, 8, 1.
- [6] T. Denning, A. Borning, B. Friedman, B. T. Gill, T. Kohno, W. H. Maisel, *CHI 2010 Conf. Proc.* ACM Press, New York, NY, USA **2010**, p. 917.
- [7] A. Cheng, L. G. Tereshchenko, *J. Electrocardiol.* **2011**, 44, 611.
- [8] M. Irimia-Vladu, *Chem. Soc. Rev.* **2014**, 43, 588.
- [9] C. J. Bettinger, Z. Bao, *Adv. Mater.* **2010**, 22, 651.
- [10] M. Bortoletti, C. Rodella, R. Salvador, P. C. Miranda, C. Miniussi, *Brain Stimul.* **2016**, 9, 525.
- [11] S. W. Hwang, H. Tao, D. H. Kim, H. Y. Cheng, J. K. Song, E. Rill, M. A. Brenckle, B. Panilaitis, S. M. Won, Y. S. Kim, Y. M. Song, K. J. Yu, A. Ameen, R. Li, Y. W. Su, M. M. Yang, D. L. Kaplan, M. R. Zakin, M. J. Slepian, Y. G. Huang, F. G. Omenetto, J. A. Rogers, *Science* **2012**, 337, 1640.
- [12] S. W. Hwang, J. K. Song, X. Huang, H. Cheng, S. K. Kang, B. H. Kim, J. H. Kim, S. Yu, Y. Huang, J. A. Rogers, *Adv. Mater.* **2014**, 26, 3905.
- [13] S. Lee, H. Wang, Q. Shi, L. Dhakar, J. Wang, N. V. Thakor, S.-C. Yen, C. Lee, *Nano Energy* **2017**, 33, 1.
- [14] D. H. Kim, J. Viventi, J. J. Arnsden, J. Xiao, L. Vigeland, Y. S. Kim, J. A. Blanco, B. Panilaitis, E. S. Frechette, D. Contreras, D. L. Kaplan, F. G. Omenetto, Y. Huang, K. C. Hwang, M. R. Zakin, B. Litt, J. A. Rogers, *Nat. Mater.* **2010**, 9, 511.
- [15] H. Wang, G. Pastorin, C. Lee, *Adv. Sci.* **2016**, 3, 1500441.
- [16] M. A. Hannan, S. Mutashar, S. A. Samad, A. Hussain, *Biomed. Eng. Online* **2014**, 13, 79.
- [17] F. R. Fan, Z. Q. Tian, Z. Lin Wang, *Nano Energy* **2012**, 1, 328.
- [18] G. H. Lim, S. S. Kwak, N. Kwon, T. Kim, H. Kim, S. M. Kim, S. W. Kim, B. Lim, *Nano Energy* **2017**, 42, 300.
- [19] S. Wang, Y. Xie, S. Niu, L. Lin, Z. L. Wang, *Adv. Mater.* **2014**, 26, 2818.
- [20] X. X. Chen, Y. Song, Z. M. Su, H. T. Chen, X. L. Cheng, J. X. Zhang, M. D. Han, H. X. Zhang, *Nano Energy* **2017**, 38, 43.
- [21] H. Ouyang, J. Tian, G. Sun, Y. Zou, Z. Liu, H. Li, L. Zhao, B. Shi, Y. Fan, Y. Fan, Z. L. Wang, Z. Li, *Adv. Mater.* **2017**, 29, 1703456.
- [22] Z. Li, G. Zhu, R. Yang, A. C. Wang, Z. L. Wang, *Adv. Mater.* **2010**, 22, 2534.
- [23] Q. Zheng, B. Shi, F. Fan, X. Wang, L. Yan, W. Yuan, S. Wang, H. Liu, Z. Li, Z. L. Wang, *Adv. Mater.* **2014**, 26, 5851.
- [24] Q. Zheng, H. Zhang, B. Shi, X. Xue, Z. Liu, Y. Jin, Y. Ma, Y. Zou, X. Wang, Z. An, W. Tang, W. Zhang, F. Yang, Y. Liu, X. Lang, Z. Xu, Z. Li, Z. L. Wang, *ACS Nano* **2016**, 10, 6510.
- [25] Y. Ma, Q. Zheng, Y. Liu, B. Shi, X. Xue, W. Ji, Z. Liu, Y. Jin, Y. Zou, Z. An, W. Zhang, X. Wang, W. Jiang, Z. Xu, Z. L. Wang, Z. Li, H. Zhang, *Nano Lett.* **2016**, 16, 6042.
- [26] F. Yi, L. Lin, S. M. Niu, J. Yang, W. Z. Wu, S. H. Wang, Q. L. Liao, Y. Zhang, Z. L. Wang, *Adv. Funct. Mater.* **2014**, 24, 7488.
- [27] P. K. Yang, L. Lin, F. Yi, X. Li, K. C. Pradel, Y. Zi, C.-I. Wu, J.-H. He, Y. Zhang, Z. L. Wang, *Adv. Mater.* **2015**, 27, 3817.
- [28] W. Song, B. Gan, T. Jiang, Y. Zhang, A. Yu, H. Yuan, N. Chen, C. Sun, Z. L. Wang, *ACS Nano* **2016**, 10, 8097.
- [29] W. Tang, J. Tian, Q. Zheng, L. Yan, J. Wang, Z. Li, Z. L. Wang, *ACS Nano* **2015**, 9, 7867.
- [30] W. B. Guo, X. D. Zhang, X. Yu, S. Wang, J. C. Qiu, W. Tang, L. L. Li, H. Liu, Z. L. Wang, *ACS Nano* **2016**, 10, 5086.
- [31] Q. Zheng, Y. Zou, Y. L. Zhang, Z. Liu, B. J. Shi, X. X. Wang, Y. M. Jin, H. Ouyang, Z. Li, Z. L. Wang, *Sci. Adv.* **2016**, 2, e1501478.
- [32] C. H. Yao, A. Hernandez, Y. H. Yu, Z. Y. Cai, X. D. Wang, *Nano Energy* **2016**, 30, 103.
- [33] C. H. Yao, X. Yin, Y. H. Yu, Z. Y. Cai, X. D. Wang, *Adv. Funct. Mater.* **2017**, 27, 1700794.
- [34] R. Z. Pana, W. P. Xuan, J. K. Chen, S. R. Dong, H. Jin, X. Z. Wang, H. L. Li, J. K. Luo, *Nano Energy* **2018**, 45, 193.
- [35] R. X. Wang, S. J. Gao, Z. Yang, Y. L. Li, W. N. Chen, B. X. Wu, W. Z. Wu, *Adv. Mater.* **2018**, 1706267.
- [36] R. A. Gross, B. Kalra, *Science* **2002**, 297, 803.
- [37] L. S. Nair, C. T. Laurencin, *Prog. Polym. Sci.* **2007**, 32, 762.
- [38] C. E. Schmidt, J. M. Baier, *Biomaterials* **2000**, 21, 2215.
- [39] S. Venkatraman, F. Boey, L. L. Lao, *Prog. Polym. Sci.* **2008**, 33, 853.
- [40] J. M. Dang, K. W. Leong, *Adv. Drug Delivery Rev.* **2006**, 58, 487.
- [41] P. B. Malafaya, G. A. Silva, R. L. Reis, *Adv. Drug Delivery Rev.* **2007**, 59, 207.
- [42] Z. L. Wang, J. Chen, L. Lin, *Energy Environ. Sci.* **2015**, 8, 2250.
- [43] G. Zhu, B. Peng, J. Chen, Q. Jing, Z. Lin Wang, *Nano Energy* **2015**, 14, 126.
- [44] A. C. Fonseca, M. H. Gil, P. N. Simões, *Prog. Polym. Sci.* **2014**, 39, 1291.
- [45] C. Zhang, W. Tang, C. Han, F. Fan, Z. L. Wang, *Adv. Mater.* **2014**, 26, 3580.
- [46] S. M. Niu, S. H. Wang, L. Lin, Y. Liu, Y. S. Zhou, Y. F. Hu, Z. L. Wang, *Energy Environ. Sci.* **2013**, 6, 3576.
- [47] S. H. Wang, L. Lin, Z. L. Wang, *Nano Lett.* **2012**, 12, 6339.
- [48] B.-M. Min, G. Lee, S. H. Kim, Y. S. Nam, T. S. Lee, W. H. Park, *Biomaterials* **2004**, 25, 1289.
- [49] B. Zuo, L. Liu, Z. Wu, *J. Appl. Polym. Sci.* **2007**, 106, 53.
- [50] X. Zhang, C. B. Baughman, D. L. Kaplan, *Biomaterials* **2008**, 29, 2217.
- [51] C. W. Hsiao, M. Y. Bai, Y. Chang, M. F. Chung, T. Y. Lee, C. T. Wu, B. Maiti, Z. X. Liao, R. K. Li, H. W. Sung, *Biomaterials* **2013**, 34, 1063.
- [52] N. Tandon, C. Cannizzaro, P. H. Chao, R. Maidhof, A. Marsano, H. T. Au, M. Radisic, G. Vunjak-Novakovic, *Nat. Protoc.* **2009**, 4, 155.
- [53] G. Eng, B. W. Lee, L. Protas, M. Gagliardi, K. Brown, R. S. Kass, G. Keller, R. B. Robinson, G. Vunjak-Novakovic, *Nat. Commun.* **2016**, 7, 10312.
- [54] J. C. Perriard, A. Hirschy, E. Ehler, *Trends Cardiovasc. Med.* **2003**, 13, 30.